Topological analysis of Hedgehog acyltransferase, a multi-palmitoylated transmembrane protein.

Antonio D Konitsiotis 1, 5,* Biljana Jovanović 1, 6, *, Paulina Ciepla 2, 3, Martin Spitaler 4, Thomas Lanyon-Hogg 2, Edward W. Tate 2, 3, and Anthony I. Magee 1, 3

1 Molecular Medicine Section, National Heart & Lung Institute, Imperial College London, Sir Alexander Fleming Building, South Kensington, London SW7 2AZ, UK
2 Department of Chemistry, Imperial College London, South Kensington, London SW7 2AZ, UK
3 Institute of Chemical Biology, Imperial College London
4 FILM Facility, National Heart & Lung Institute, Imperial College London, Sir Alexander Fleming Building, South Kensington, London SW7 2AZ, UK
5 Current address: Max Planck Institute of Molecular Physiology, Department of Systemic Cell Biology, Otto-Hahn-Str. 11, 44227 Dortmund, Germany.
6 Current address: Department of Biosciences and Nutrition, Karolinska Institutet SE-141 57 Huddinge, Sweden
* Authors contributed equally to this work.

Running title: Topological analysis of HHAT

Joint corresponding authors: Anthony I. Magee, Molecular Medicine Section, National Heart & Lung Institute, Imperial College London, South Kensington Campus, London SW7 2AZ, UK. Tel: +44 (0)20 7594 3135. E-mail: t.magee@imperial.ac.uk
Edward W. Tate, Department of Chemistry, Imperial College London, South Kensington, London SW7 2AZ, UK. Email: e.tate@imperial.ac.uk

Keywords: topology; acyltransferase; MBOAT; click-chemistry; cancer

Background: Hedgehog acyltransferase (HHAT) palmitoylates hedgehog proteins and is a potential target in cancer.
Results: HHAT has 10 transmembrane domains, 2 reentrant loops and 4 palmitoylation sites.
Conclusion: HHAT topology is determined and protein is multi-palmitoylated, which modulates protein function.
Significance: Elucidating HHAT topology and post-translational modifications is crucial to understanding its acyltransferase activity and in developing new strategies to treat cancer.

ABSTRACT

Hedgehog proteins are secreted morphogens that play critical roles in development and disease. During maturation of the proteins through the secretory pathway they are modified by the addition of N-terminal palmitic acid and C-terminal cholesterol moieties, both of which are critical for their correct function and localisation. Hedgehog acyltransferase (HHAT) is the enzyme in the endoplasmatic reticulum (ER) that palmitoylates Hedgehog proteins, is a member of a small subfamily of MBOAT proteins that acylate secreted proteins, and is an important drug target in cancer. However little is known about HHATs structure and mode of function. We show that HHAT is comprised of 10 transmembrane domains and 2 reentrant loops with the critical His and Asp residues on opposite sides of the ER membrane. We further show that HHAT is palmitoylated on multiple cytosolic cysteines, which maintain protein structure within the membrane. Finally, we provide evidence that mutation of the conserved His residue in the hypothesised catalytic domain results in a complete loss of HHAT palmitoylation, providing novel insight into how the protein may function *in vivo*.

INTRODUCTION

The Hedgehog (Hh) family of proteins are secreted morphogens which play a significant role during embryonic development in determining organogenesis and anterior-posterior patterning of various tissues, including the central nervous system and limb and digit formation (1,2). Aberrant activation of Hh signaling in various cancers result in promotion of cancer growth and metastasis (3,4) and small

molecule inihbitors for this pathway are in use in various clinical trials.

A unique feature of the Hh proteins are that during maturation through the secretory pathway, they are post-translationally modified by the addition of a cholesterol moiety to its C-terminus, via an ester linkage, while a palmitate (C16:0) fatty acid is also added on the conserved N-terminal cysteine residue via an amide linkage (5). Palmitoylation of Hh proteins is catalysed by the protein acyltransferase (PAT) Hedgehog acyltransferase (HHAT) (6).

These modifications produce the mature and functional Hh signaling molecule and are crucial for the correct function of the protein. They not only direct the formation of large Hh multimers upon secretion from the producing cells, but they also determine the proper release and targeting of the proteins, as well as having a significant effect on the potency of the protein to activate the signaling pathway on the receiving cells (7-9). For these reasons, disrupting the post-translational modification of Hh proteins, and hence inhibiting the formation of functional signaling molecules, is an attractive new method of inhibiting the Hh pathway in cancer.

HHAT is a multipass transmembrane (TM) domain protein located in the endoplasmic reticulum (ER) of cells (6,10), and a member of a small sub-group of the membrane-bound O-acyltransferase (MBOAT) superfamily of proteins, that specifically acylates secreted proteins.. Other members of this important sub-group include Porcupine (PORCN) which palmitoyleoylates (C16:1) the Wnt family of proteins and ghrelin-O-acyltransferase (GOAT) which octanoylates (C8:0) the appetite-sensing peptide ghrelin (11). All MBOAT proteins are characterized by their MBOAT homology domain, a region of highly conserved residues including an invariant His residue (His379 in the case of HHAT) and a highly conserved Asn - or in the case of HHAT, Asp (Asp339) - residue 30-45 amino acids upstream (11,12). These amino acids are proposed to be catalytic, although this is still not clear, especially for HHAT where mutation of the His to an Ala still retains significant PAT activity (13). Recent studies by our group and others provided proof of principle that inhibiting HHAT function is a valid method of inhibiting Hh signaling in cancer (14-16).

Despite the importance of HHAT in Hh signaling and its therapeutic potential in cancer, little is understood about the structure of the protein and the identity of the catalytically important amino acids, information that may guide future studies in development of small molecule inhibitors of HHAT as well as into other functions HHAT may have in the cell. In this study, we determine HHAT topology using a variety of experimental methods. Our data suggest that HHAT contains 10 TM domains and 2 re-entrant loops (RLs) and that the invariant His379 is luminal, while Asp339 is on the cytosolic side of the ER. Furthermore, we show that HHAT is itself palmitoylated at multiple cytoplasmic Cys residues, and His379 is critical for the palmitoylation of HHAT, while a conserved Cys324 appears to modulate protein topology significantly.

EXPERIMENTAL PROCEDURES

Cell culture and transfection - HEK293a and HeLa cells were cultured in high glucose (4.5g/L) DMEM supplemented with Glutamax (Life Technologies, Paisley, UK) containing 10% foetal bovine serum (FBS, Sigma, Gillingham, UK). All cells were grown at 37 °C in a humidified incubator under 5% CO_2. Cells were transfected at 70% confluence using Turbofect (Thermo Fisher Scientific, Cramlington, UK) according to the manufacturer's specifications.

Plasmid construction and mutagenesis - Full-length human HHAT cDNA (Accession No: BC117130) expression vector with C-terminal V5 and 6xHis epitopes has previously been described (15). The cloned cDNA sequence carries a missense mutation compared to the human *HHAT* consensus sequence, a serine to aspartate change in position 182 of the protein. Prior to proceeding with making mutants for HHAT for topology analysis, the missense mutation was corrected to serine by QuickChange II site-directed mutagenesis (forward primer: CTACTACACCAGCTTCAGCCTGGAGCTCT GCTGGCAGCAGC; reverse primer: CAGGCTGAAGCTGGTGTAGTAGAGGCAG CGAACGGTCAGCG). All subsequent HHAT mutants and truncates for topological analysis were made using the corrected vector expressing HHAT-V5-Hisx6 as template.

For cysteine mapping topology analysis, selected cysteines were mutated to alanine by Q5 site-directed mutagenesis (NEB, Hitchin, UK). Q5 mutagenesis was also used for the introduction of the TEV protease site, ENLYFQG, in the HHAT-TEV mutants.

For the production of the V5 topology clones, the V5-6xHis epitope from the HHAT-V5-6xHis construct was removed and replaced with a FLAG epitope (DYKDDDDK) by Q5 mutagenesis, followed by insertion of the V5 epitope (GKPIPNPLLGLDST) at the required sites.

For *N*-glycosylation analysis, an *N*-glycosylation site (Asp-Leu-Thr) was introduced by QuickChange II site-directed mutagenesis into the spacer region between the gene of interest cloning site and the V5-Hisx6 epitope of the empty destination vector pcDNA-DEST40 used for HHAT cloning Next, full length HHAT or HHAT truncations HHAT-Δ157-493 and HHAT-Δ192-493 were amplified from the HHAT expression vector described above (15) and cloned into the modified destination vector using Gateway cloning resulting in expression vectors carrying *N*-glycosylation, V5 and Hisx6 epitopes at the C-terminus. All clones were verified by sequencing.

SDS-PAGE and immunoblotting - Separation of proteins was performed by sodium dodecyl sulphate-polyacrylamide gel electrophoresis (SDS-PAGE), using 10 or 15% Tris gels and Tris-glycine-SDS running buffer. Samples were prepared in NuPAGE® LDS 4 x sample loading buffer (Life Technologies) and 10% (v/v) 2-mercaptoethanol (unless stated otherwise). The protein ladder used for comparison of molecular weight was Precision Plus Protein® Standards All Blue (Bio-Rad, Herts, UK). Gels were run using the Mini-PROTEAN® Tetra Cell System and power supply unit (Bio-Rad). Fluorescently-tagged proteins were imaged (540 nm excitation and 595 nm emission, channel Cy3) using an Ettan DIGE Imager (GE Healthcare, Bucks, UK) and images were analysed with ImageQuantTM TL software (GE Healthcare).

Proteins were transferred from SDS-PAGE gels to a PVDF membrane (Millipore, UK) using a semi-dry transfer unit (Hoefer, Holliston, MA, USA). Membranes were blocked with blocking solution (5% w/v milk powder (Marvel), dissolved in PBS) for 1 h at room temperature and washed with PBS-T (phosphate buffered saline, PBS, containing 0.05% Tween-20 (Sigma)) and probed with appropriate antibodies. Antibodies and their sources were as follows: mouse anti-V5 monoclonal antibody (1:10,000 dilution, Life Technologies); mouse anti-6xHis antibody (1:1000, AD1.1.10, R&D Systems, Abingdon, UK), rabbit anti-6xHis antibody (1:1000, ab137839, Abcam, Cambridge, UK); goat anti-Grp94 antibody (1:200 dilution, C-19, Santa Cruz Biotechnology, UK); anti-calnexin-N-terminus mouse monoclonal IgG1 (1:1000, AF18, Sigma). Secondary antibodies used were: goat anti-mouse IgG2a-HRP (1:20,000 dilution, Southern Biotech, UK); goat anti-mouse IgG1-HRP (1:20.000, Southern Biotech); goat anti-rabbit-HRP IgG (1:20,000, Southern Biotech); or after immunoprecipitations, mouse anti-rabbit IgG-HRP VeriBlot (1:1000, Abcam, UK).

Visualisation was carried out by enhanced chemiluminescence kit (Pierce ECL2 Western Blotting Substrate, Thermo Scientific, UK) according to manufacturer's instructions and on an Ettan DIGE Imager (GE Healthcare, UK), excitation at 480 nm, emission at 530 nm (channel Cy2). Images were analysed with ImageQuantTM TL software.

TEV cleavage of ER microsomes - HEK293a cells were transfected with wild-type or TEV mutant HHAT-V5-6xHis constructs. After 48 h, cells were washed twice with cold HCN buffer (50 mM Hepes, pH 7.5, 150 mM NaCl, 2 mM $CaCl_2$) and pelleted at 800 × g for 2 min. Cells were passed through a 23g needle 10 times and then intact cells and nuclei were pelleted at 800 x g for 5 min at 4^{o}C. The supernatant was then ultracentrifuged at 100,000 x g for 1 h to obtain microsomes, which were resuspended in ProTEV protease buffer (50mM HEPES pH 7.0, 0.5mM EDTA, 1mM DTT) and protein concentration determined using the DC protein assay (BioRad). Due to lower expression levels of some mutants, an initial Western Blot was performed on 5μg of each microsome preparation in order to determine the amount of HHAT expression. The final concentration of microsome preparation treated with ProTEV was then normalised for HHAT expression. To every 20μg of microsome suspension 1μl (5U) of ProTEV Plus protease (Promega, Southampton, UK) was added and then preparations were incubated at 25°C for 4 h. Reaction was stopped with NuPAGE® LDS 1 x sample loading buffer (Life Technologies). Proteins were then separated by SDS-PAGE and analysed by immunoblotting with anti-V5 monoclonal antibody (1:10,000 dilution, Life Technologies). After probing for V5, blots were re-probed with anti-6xHis (1:1000, AD1.1.10, R&D Systems) antibody.

Metabolic labelling with alkynyl-palmitate (YnPalm) and Copper-catalyzed [3+2]

cycloaddition (CuAAC) reaction - HEK293a cells were transfected with wild-type or cysteine-mutant HHAT-V5-6xHis constructs. 36 h post-transfection, medium was exchanged for feeding medium (DMEM, 3% FBS plus 50 μM alkynyl-palmitate analogue pentadec-14-ynoic acid (YnPalm) in DMSO(17), or the same volume of DMSO used as vehicle control . After 16 h, cells were rinsed twice with ice-cold PBS and then lysed with 100μl lysis buffer (0.1% SDS, 1% Triton X-100, EDTA-free Complete protease inhibitor (Roche Diagnostics, Burgess Hill, UK) dissolved in PBS). Lysates were centrifuged at 16,000 x g for 10 min to remove insoluble material. The supernatant was collected and used for further experiments.

Cell lysates (20 μg of total proteins) were reacted with CuAAC reaction cocktail containing azido-TAMRA-PEG-Biotin (AzTB) (10 mM stock in DMSO) at 100 μM final concentration(17), $CuSO_4$ (50 mM stock in water) at final concentration of 1 mM, TCEP (50 mM stock in water) at final concentration of 1 mM and TBTA (10 mM stock in DMSO) at final concentration of 100 μM. The reaction was vortexed for 1 h at room temperature and EDTA (100 mM in water stock) was added to final concentration of 10 mM. Proteins were precipitated by addition of 4 vols of methanol, 1 vol of chloroform and 3 vols of water. The sample was centrifuged for 5 min at 16,000 x g and the pellet was washed twice with room temperature (RT) methanol. The protein precipitates were resuspended in 2% SDS in PBS and further diluted to 1 mg/mL of total protein concentration and final SDS concentration of 0.2% with PBS. An aliquot of this sample was taken for SDS-PAGE analysis.

200 μg of proteins from cell lysate were immunoprecipitated with 1 μg anti-V5 antibody. Following overnight incubation at 4°C on a rotating wheel, 25 μL of Pureproteome protein-G magnetic beads (Merck Millipore, Watford, UK) were added to each sample and incubated for 1 h at 4 °C on a rotating wheel. The beads were washed (5 x) with lysis buffer and resuspended in 20 μL of PBS and freshly premixed CuAAC reaction reagents at appropriate concentrations (as described above) were added. After 1 h of vortex-mixing, the beads were washed (5 x) with lysis buffer and mixed with NuPAGE® LDS 1 x sample loading buffer (Life Technologies) and 10% (v/v) 2-mercaptoethanol and incubated with vortexing at room temperature for 1 h. Proteins were separated by SDS-PAGE, in-gel fluorescence was used to visualise YnPalm-modified proteins, which were then transferred to PVDF membranes and analysed by immunoblotting with anti-6xHis (1:1000, ab137839, Abcam) antibody followed by mouse anti-rabbit IgG (HRP) VeriBlot (1:1000, Abcam) secondary antibody.

Hydroxylamine (NH_2OH) treatment of YnPalm-modified proteins - After preparation of lysates from metabolic labelling of palmitoylated proteins with YnPalm (see section above) lysates were diluted 1:1 with 2M NH_2OH pH 7.5 or 2M Tris pH 7.5. Samples were then incubated for 5 h at RT while mixing with a rotator wheel. HHAT proteins were then immunoprecipitated onto protein G magnetic beads with anti-V5 antibody and treated by CuAAC, as described above. Proteins were separated by SDS-PAGE, in-gel fluorescence was used to visualise YnPalm-modified proteins, which were then transferred to PVDF membranes (Millipore) and analysed by immunoblotting with anti-6xHis antibody.

mPEG labelling of cells - HEK293a cells were transfected with wild-type or cysteine mutant HHAT-V5-6xHis constructs. After 48 h, cells were washed twice with ice-cold HCN buffer, and pelleted at 800 × g for 2 min. Cells were then semipermeabilised in 0.02% digitonin or fully permeabilised in 1% Triton X-100 on ice for 20 min (in HCN buffer supplemented with a protease inhibitor cocktail). In the experiments with microsomal fractions, 20μg of microsomal fractions in cold HCN buffer with or without 0.2% Triton X-100 were used. 1mM maleimide-polyethyleneglycol (mPEG) 5 kDa (Laysan Bio Inc, AL, USA) was then added to each sample with or without 20 mM DTT for 30 min on ice, after which all samples were brought to a final concentration of 1% TX-100/20 mM DTT and incubated an additional 15 min on ice. Lysates were clarified by spinning at 16,000 × g for 10 min and the proteins in the supernatants were separated by SDS-PAGE. Samples were analysed by immunoblotting with anti-V5, anti-6xHis or anti-Grp94 (1:200 dilution, C-19, Santa Cruz Biotechnology, UK) antibodies.

HHAT V5-topology determination - Topology determination by V5 accessibility was performed as follows: 1.5 x 10^4 HeLa cells were plated on 96-well imaging plates (ibidi) and transfected with wild-type or mutant HHAT-V5-FLAG constructs. After 48 h, cells were fixed with 3% paraformaldehyde (PFA) in PBS pH 7.5

for 10min at room temperature, washed thoroughly and then semipermeabilised in 0.02% digitonin/PBS or fully permeabilised in 0.2% Triton X-100/PBS on ice for 10 min. HHAT was visualised with mouse monoclonal anti-V5 IgG2A (1:300, Life Technologies) and rabbit polyclonal anti-DDDDK (1:300, ab1162, Abcam) followed by AlexaFluor488-conjugated anti-mouse IgG2A and AlexaFluor555-conjugated anti-rabbit secondary antibodies (Life Technologies), respectively. As a control for the permeabilisation of the cells, untransfected cells treated in the same way as the HHAT-transfected cells were stained for calnexin using two different antibodies, one against the N-terminus of the protein, mouse monoclonal IgG1 (AF18, 1:50, Santa Cruz), and one against the C-terminus, rabbit polyclonal (ADI-SPA-860, 1:100, Enzo Life Sciences), followed by AlexaFluor488-conjugated anti-mouse IgG1 and AlexaFluor555-conjugated anti-rabbit secondary antibodies, respectively. Imaging was performed using a Zeiss Axiovert 200 widefield microscope with a LD Achroplan 40x 0.60 KORR Ph2 objective and Hamamatsu OrcaER CCD camera in the FILM imaging facility. Colocalisation analysis was performed using Volocity image analysis software (PerkinElmer, Cambridge, UK). The two channels were thresholded by drawing a region of interest (ROI) in a background area of the image. The mean intensity of the region for each channel was calculated and this was set as the lower threshold. ROIs were then drawn around the ER regions of transfected cells and then the Manders colocalisation coefficient was determined. Images from at least 40 cells from 3 independent experiments were used in the analysis.

In vitro expression of HHAT N-glycosylation mutants - *In vitro* protein expression of full length HHAT, HHAT-Δ157-493 and HHAT-Δ192-493 truncations containing a C-terminal N-glycosylation motif was performed using the TnT Quick Coupled Transcription/Translation System (Promega) based on rabbit reticulocyte lysate with canine pancreatic microsomes. 40 µl TnT master mix, 1 µg plasmid template, 1 µl methionine (1 mM), and 3.6 µl canine pancreatic microsomes were mixed on ice. Volume was adjusted to 50 µl with RNase-free water and reactions were incubated at 30°C for 1.5 h.

Removal of protein N-glycosylation by treatment with PNGase F - After *in vitro* protein transcription and translation, microsomal membranes were purified by diluting the components of the TnT reaction to 500 µl in PBS and carefully layered on top of 100 µl of 5% (w/v) sucrose in 1.5 ml tubes for ultracentrifugation (Beckman). The samples were centrifuged at 100,000 × *g* for 45 min at 4°C to pellet the membranes. Supernatant was discarded, membrane pellet was resuspended in 10 µl of glycoprotein denaturing buffer supplied with the PNGase F kit (NEB) and heated at 100°C for 10 min. The samples were incubated at 37°C for 1 h with or without PNGase F (according to manufacturer's instructions). The reactions were stopped by addition of 4× NuPage LDS sample buffer (Invitrogen) and analysed by immunoblotting against the V5 epitope.

Shh in vitro click-chemistry based palmitoylation assay - Details of our Shh in vitro click-chemistry based palmitoylation assay will be reported fully elsewhere (T. Lanyon-Hogg, A.I. Magee and E.W. Tate, in preparation). Briefly, Shh residues 1-11 were synthesised by solid phase peptide synthesis attached to a C-terminal (PEG)-biotin tag. YnPalm-CoA was synthesised from YnPalm and Co-enzyme A hydrate from yeast (Sigma) using standard 1,1'-carbonyl-diimidazole coupling conditions. HEK293a cells were transfected with HHAT-V5-6xHis (positive control), HHAT-H379A-V5-6xHis, HHAT-D339N-V5-6xHis, or mCherry (negative control) and grown to 70 % confluency. Cells were lysed as previously described and membrane fractions collected via centrifugation at 100,000 x g for 1 h at 4 °C. Membrane fractions were solubilised in solublisation buffer (1% (w/v) n-Dodecyl β-D-maltoside, 10 mM HEPES (pH 7.5), 350 mM NaCl) for 1 h at 4 °C, and insoluble material removed by centrifugation at 100,000 g for 1 h at 4 °C. Solubilised HHAT-H389A and -D339N membrane fractions were normalised to HHAT-WT expression levels via α-6xHis immunoblotting, and 3 µg HHAT-WT or mCherry membrane fractions were used for in vitro palmitoylation. 1 µM YnPalm-CoA and 1 µM Shh(1-11)-biotin in reaction buffer (100 mM MES (pH6.5), 20 mM NaCl, 1 mM DTT, 0.1% (w/v) BSA) were incubated with solubilised membrane fractions for 30 min at RT in Reacti-Bind Streptavidin coated clear wells (Fisher). Wells were washed with 3 x 200 µl PBS-T + 1% BSA, followed by 3 x 200 µl reaction buffer. Wells were then subjected to CuAAC click-chemistry functionalization with 10 µM azido-

FLAG peptide, 1 mM CuSO4, 1 mM TCEP, 1 mM TBTA in PBS-T + 0.1% BSA for 1 h at RT, then washed with 3 x 200 µl PBS-T + 1% BSA, followed by 3 x 200 µl reaction buffer. Wells were probed with α-FLAG-HRP (Sigma) (1:20,000) in PBS-T + 0.1% BSA for 1 h at RT, then washed with 3 x 200 µl PBS-T + 1% BSA, followed by 3 x 200 µl reaction buffer. Bound α-FLAG-HRP (Sigma) was visualised using BD OptEIA TMB reagent (Becton Dickinson) according to the manufacturer's protocol, and wells read for optical density at 450 nm. Samples were prepared in duplicate and the experiment was repeated twice.

RESULTS

Bioinformatic analysis of HHAT topology - There are 7 human HHAT isoforms (UniProt ref: Q5VTY9); however, the canonical polypeptide sequence is isoform 1, which is 493 amino acids long. Topology for this isoform has been previously predicted using TMHMM 2.0 (18) to have 8 transmembrane (TM) helices (13). This model, however, had a number of inconsistencies in comparison to other MBOAT protein topologies, most significantly that the critical His379 of the conserved MBOAT region of HHAT was predicted to be cytosolic, a feature that would be unique within this family of proteins and seems inconsistent with catalytic activity on Hh proteins in the ER lumen. A recent comparison of different topology prediction algorithms identified some as being superior for predicting structures of membrane proteins (19); the highest-scoring topology prediction algorithm was TOPCONS (20). Furthermore, the study that recently determined the topology of GOAT (21) utilised an advanced algorithm MEMSAT-SVM (22) which employs a computer learning method, as well as considering extra features, such as RLs and signal peptides.

We performed topology predictions for HHAT sequences from 22 different species, identified on the NCBI RefSeq database (Figure S1) (23) using both the TOPCONS and MEMSAT-SVM prediction algorithms (data for human HHAT sequence shown in Figure 1, data for other species not shown). Significantly, both prediction algorithms gave very similar results and were internally consistent across different species, with models predicted to contain either 11 or 12 TM domains in both algorithms.

Loop 8 was the longest and another algorithm TMpred (24) predicted an intervening TM, although with a low score; the other predicted TMs were similar to the TOPCONS and MEMSAT-SVM predictions (Figure 1). TMpred predicts protein topology through several weight-matrices based on the statistical analysis from a SWISS-PROT TM protein database (release 25). To test this prediction in our experiments we made two mutants within loop 8 (numbered 8 and 8b) for all experiments.

In all sequences analysed, no N-terminal cleavable signal peptide was predicted either by MEMSAT-SVM or SignalP 4.0 (25). This was also confirmed experimentally (see below). Finally, in all topologies, the critical His379 residue is predicted to be on the luminal side of the membrane at the border between predicted TM9 and loop 10.

HHAT topology determination by Tobacco Etch Virus (TEV) protease protection assay on purified ER microsomes - Based on the predicted topology of human HHAT, a number of constructs were designed containing TEV protease recognition sites (ENLYFQG) within predicted loops, which also contained a V5-6xHis epitope tag on the C-terminus of the protein; the insertion sites are indicated in Figure 1. TEV protease is a highly site-specific cysteine protease from Tobacco Etch Virus. The optimum recognition sequence is ENLYFQ|G and cleavage occurs between the Gln and Gly residues.

We isolated intact microsomes containing ER membranes from cells expressing HHAT-TEV constructs and treated these preparations with ProTEV protease *in vitro* (Figure 2). We first confirmed that the ER membrane was intact by checking the ability of the thiol-reactive reagent mPEG to modify the non-disulphide-bonded cysteine in the ER luminal protein GRP94 (Figure 2A) (26). Isolated microsomes treated with mPEG had only a single GRP94 band at ~100kDa (Figure 2A - upper blot). However, if 0.2% Triton X-100 was added during mPEG treatment to permeabilise the membrane, a second mPEG-modified band appears (Figure 2A - middle blot) and this band disappears if treated at the same time with 20mM DTT, which competes with mPEG reacting with the cysteine in GRP94 (Figure 2 A - lower blot). Having confirmed that the microsomes are intact, we proceeded with protease treatment.

Protein levels were adjusted to achieve equal levels of mutant HHAT expression and the amount of ProTEV protease was adjusted for protein concentration (see Experimental

Procedures). In the absence of ProTEV protease (Figure 2B-I and 2C-I) all HHAT constructs migrated as single ~50kDa bands; however, with the addition of ProTEV additional bands appeared, indicating successful cleavage of some of the HHAT-TEV constructs. This is particularly apparent from the sizes of these additional bands, which correspond to the expected size of tagged C-terminal peptides produced on cleavage of the proteins. Thus, proteins with TEV sites in loops close to the N-terminus of the protein produce larger cleavage products than proteins with TEV sites close to the C-terminus of the protein. Using this approach we were able to verify that loops 4, 6, 8 and 10 were cytosolic (Figure 2B-II, 2C-II). Cleavage products indicated with black arrowheads), while the C-terminus of the protein was also cytosolic, as a HHAT-TEV construct in which the TEV recognition sequence was placed between the C-terminal V5 and 6xHis epitopes showed a loss of α6xHis immunoreactivity (Figure 2D). Mutants HHAT-3 TEV and HHAT-8b TEV showed the appearance of a band in the presence of TEV, but because of background bands obscuring the clear appearance of the cleaved product we are unable to determine the loop topology reliably (Figure 2B-II, 2C-II, potential cleavage products indicated with grey arrowheads). Loops 5, 7, 9 and 11 showed no evidence of TEV cleavage and therefore appear to be luminal. With regard to the first two loops of the protein, because of the size of the cleavage products coinciding with the size of ProTEV and the relatively lower immunoreactivity of the cleavage products using the anti-V5 antibody (Compare Figure 2B-II and 2C-II) it was not clear if the protein was cleaved. All mutants cleaved when cells were fully permeabilised with dodecyl maltoside, showing that the cleavage sites were functional (data not shown). These experiments are consistent with a 10 TM model for HHAT topology with 2 RLs (RL3 and RL6) and a cytosolic C-terminus (Figure 2C-II, diagram beneath blot).

HHAT mapping by epitope immunoreactivity in selectively permeabilised cells - We wanted to complement the results obtained with TEV protease mapping with an alternative method, ideally in a cellular context and in such a manner that would give a definite result for loops near the termini of HHAT, as well as for the N- and C-termini themselves. We decided to pursue an epitope mapping strategy in selectively permeabilised cells using indirect immunofluorescence. We generated HHAT constructs that were C-terminally tagged with a FLAG tag (DYDDDDK) and had a V5 epitope (GKPIPNPLLGLDST) inserted at the same points at which the TEV protease site had been inserted, as well as an N-terminal V5-tagged version (see Figure 1). HeLa cells expressing these constructs were fixed and treated with 0.2% Triton X-100 to fully permeabilise the cell membranes, or treated with 0.04% digitonin, which selectively permeabilises the plasma membrane of the cells but leaves the ER membrane intact (21,26). Cells were then stained for both FLAG and V5 epitopes by indirect immunofluorescence (Figure 3). As a control for the permeabilisation protocol, cells were stained with two different Calnexin antibodies, one which recognises the N-terminus of the protein and another which recognises the C-terminus of the protein. Calnexin is a type I transmembrane domain protein which is abundant in the ER and functions as a chaperone for secretory glycoproteins (27), the N-terminus of which is luminal and the C-terminus cytoplasmic (28); thus in digitonin-treated cells, the N-terminus specific antibody should not react with the protein, but the C-terminus specific antibody should react regardless of treatment (Figure 3-I). Similar analysis was performed using the HHAT-V5-FLAG constructs in permeabilised and semi-permeabilised cells (data for two mutants shown in Figure 3-II and -III). Images were collated from at least three separate experiments and Manders' correlation coefficient was calculated for each mutant in the digitonin-treated condition to determine if the two probes were on the same side of the ER membrane (Figure 3-IV).

As expected from the TEV experiments, the C-terminus of HHAT was cytosolic for all HHAT constructs; this also confirmed that none of the insertions caused the TMs to flip (Figure 3 and data not show). The N-terminus was also cytosolic, as predicted by both TOPCONS and MEMSAT-SVM (Figure 3-II). The staining also confirmed that the protein does not contain an N-terminal cleavable signal peptide, as the V5 tag would have been removed in that case. The results for the other mutants correspond mostly, but not completely, to the TEV protease experiments. Specifically, loops 2, 3, 5, 6, 8 and 10 all appeared to be cytosolic, while loops 1, 4, 7, 9 and 11 were luminal (see schematic in Figure 5). In the case of the loop 9 mutant we

decided to make a second mutant in which the V5 epitope was shifted C-terminally by three amino acids (HHAT-9b V5-FLAG), in order to correct for any potential masking of the epitope from being in close proximity to a predicted TM domain; however, results still suggested the loop was luminal. The results of the epitope mapping showed very good overlap with the TEV experimental model. Noteworthy exceptions were loops 4 and 5, which the TEV experiments place as cytosolic and luminal, respectively, while in the epitope mapping the opposite orientation is seen.

To resolve this discrepancy, C-terminal truncation mutants of HHAT containing the first four or five predicted TMs of HHAT and a C-terminal N-glycosylation motif followed by the V5-6xHis epitope were constructed and expressed by *in vitro* translation in the presence of microsomes. Lysates were then analysed by Western blotting to see if the C-terminus of the protein was glycosylated or not (Figure 4. This method supported a luminal location for loop 4, and a cytosolic location for loop 5 thus confirming the V5 epitope mapping result (Figure 3-IV). We also confirmed in the same way that the C-terminus of full length HHAT is cytosolic (Figure 4).

Based on the TEV protease mapping, the epitope mapping on selectively permeabilised cells and the glycosylation of HHAT truncations, a consensus topology model can be drawn up in which HHAT has 10 TM domains and 2 RLs (RL3 and RL6; Figure 5), while His379 is close to the luminal side of the ER and Asp339 was cytosolic.

Cytoplasmic cysteine accessibility suggests cysteine modification and a stabilising role for Cys324 - HHAT has 14 cysteines and, based on the consensus experimental topological model of HHAT described above (Figure 5), HHAT is predicted to have three luminal cysteines, C126-C139-C282, and four cytosolic cysteines, C188-C242-C324-C410, while the rest of the cysteines are embedded in the hydrophobic core of the membrane.

In order to examine this prediction, we transfected cells with the wild type HHAT-V5-6xHis construct and either fully permeabilised the cells with 1% Triton X-100 or semi-permeabilised the cells with 0.04% digitonin, and treated the cells with mPEG (Figure 6A). The ER membrane was intact in digitonin-treated cells, as GRP94 was not modified. Surprisingly, in fully permeabilised cells there was only a SDS-PAGE shift of HHAT-V5-6xHis corresponding to ~15kDa (analysis on 4 experiments indicate a shift of 14.1 +/- 0.84 kDa) indicating that only 3 cysteines had been modified by mPEG (which has a molecular weight of ~5kDa). Even more surprisingly, in the semi-permeabilised cells, no band shift was seen, indicating that all three tagged cysteines were luminal. This supports our hypothesis that three cysteines of HHAT would be in the lumen of the ER, but raised a question as to why no cytosolic cysteines were accessible.

It is possible that cytosolic cysteines are not accessible to mPEG through steric hindrance from the secondary, tertiary or quaternary structure of the cytosolic loops. Another possibility is that the –SH groups of the cysteines are not available to react with mPEG because of another modification or formation of a disulphide bond with neighbouring cysteines, although this is unlikely for cytosolic cysteines due to the reducing environment of the cytoplasm. This was also excluded by running HHAT on non-reducing gels, in which we did not see altered mobility which would be evidence of disulphide bond formation (data not shown). Thus, either the cysteines were inaccessible or they were modified in some other way.

We performed an alanine scan of all cysteines followed by mPEG labelling in fully permeabilised cells in order to see if we could identify the cysteines that were being labelled with mPEG (Figure 6B). None of the single cysteine mutations resulted in a quantifiable reduction of the mPEG modification of HHAT. Unusually, the cysteine mutant C324A when tagged with mPEG gave rise to multiple bands of increasing size (Figure 6B, lane 10 in right hand blot and 6C), suggesting that by mutating this single cysteine, other cysteines within the protein somehow become accessible and/or multimer formation is promoted.

HHAT is palmitoylated on multiple cytoplasmic cysteines - The inaccessibility of HHAT cytosolic cysteines to the mPEG alkylating reagent and the lack of disulphide bonds in the protein suggested that the cysteines are perhaps modified in some other way. We hypothesised that HHAT is palmitoylated, partly based on studies showing that the DHHC PATs form an auto-acylated intermediate (29) before acylating their substrate proteins. Furthermore, cytosolic juxtamembrane cysteines of transmembrane proteins are frequently palmitoylated.

Therefore, we decided to examine if HHAT was acylated.

HEK293a cells overexpressing human HHAT-V5-6xHis were metabolically labeled with YnPalm (alkynyl-palmitate analogue pentadec-14-ynoic acid) (17), cells were lysed and HHAT was immunoprecipitated via it's C-terminal V5 tag onto protein G beads. Precipitated proteins were then subjected to CuAAC ligation to azide-containing trifunctional capture reagent azido-TAMRA-PEG-Biotin (AzTB) (17). Proteins were separated by SDS-PAGE and palmitoylated proteins were then identified by in-gel fluorescence (upper panels) and verified by anti-6xHis immunoblotting (lower panels) (Figure 7A). As is seen in the input samples (upper left panel) there are multiple bands, corresponding to all the proteins in the palmitoylome of the cell; however, after V5 immunoprecipitation (upper right panel) a major band is visible at 50kDa corresponding to palmitoylated HHAT. Furthermore, treatment of the lysates with hydroxylamine (NH_2OH) at neutral pH, which cleaves thioester bonds, before V5 pull-down and CuAAC ligation, led to a loss in HHAT palmitoylation signal (Figure 7B), confirming that HHAT is palmitoylated via a thioester bond on at least one cysteine residue.

We used the cysteine-to-alanine mutants discussed above in similar metabolic labelling experiments and in Acyl-RAC pulldown experiments (30). However, no single cysteine resulted in significant decreased pulldown, suggesting that multiple cysteines were being acylated (data not shown).

Based on our experimentally determined topology of HHAT (Figure 5), four cysteines, C188-C242-C324-C410, are expected to be on the cytosolic side of the ER membrane, where palmitoylation by DHHC PATs is expected to occur. We made two multiple cysteine-to-alanine mutants, in which either all four cysteines were mutated to alanine (4CysA), or just three of the cysteines were mutated (3CysA), leaving out Cys188 which is predicted to be within a re-entrant loop and so may not be accessible to mPEG modification (see section above). These mutants were metabolically labelled with YnPalm and analysed by anti-V5 precipitation and CuAAC ligation to AzTB (Figure 7C). In the HHAT-3CysA mutant, there was a decrease in palmitoylated HHAT signal, although a faint band was still visible in the in-gel fluorescence (see Figure 7C; gel on the right, compare lane 4 with lane 8). However, mutation of all four cysteines to alanine in the HHAT-4CysA mutant, led to a complete loss of YnPalm signal (compare lane 4 with lane 10), indicating that all four cysteines on the cytosolic side of the protein are palmitoylated. Significantly, a mutant protein in which all the predicted luminal cysteines were mutated to alanine, HHAT-LumCys mutant, was still palmitoylated to an equal extent as the wild type protein (compare lane 4 with lane 6).

Finally, we examined if HHAT activity was important for its palmitoylation. The HHAT mutants D339N and H379A have significantly reduced activity (13), with D339N showing a severe loss of activity while H379A retained ~60% activity of WT HHAT (Figure 8A). HEK293a cells overexpressing HHAT-D339N or HHAT-H379A were metabolically labelled with YnPalm and HHAT palmitoylation was examined by in-gel fluorescence (Figure 8B). These experiments showed that HHAT-D339N was still palmitoylated; however, HHAT-H379A was only weakly palmitoylated, indicating that the conserved His379 residue of the MBOAT region of HHAT is important for the palmitoylation of HHAT and that this may be critical for HHAT function.

DISCUSSION

In this study we have determined the topology of HHAT by TEV protease and V5 epitope mapping in microsome preparations and selectively permeabilised cells, respectively. While, we also have shown that HHAT is multi-palmitoylated, which may affect protein function.

The model we have developed (Figure 5) consists of 10 TMs and 2 RLs, with cytosolic N- and C-termini, and the conserved His379 residue from the MBOAT domain being at the lumenal tip of TM-9 and the critical Asp339 in a large cytosolic loop, which contains a palmitoyalted Cys. This model is significantly different from the previously proposed model, which consisted of 8TMs, and the His and Asp residues were in a single large cytosolic loop (13). Our experimentally validated model shows a good correlation with the predicted topologies of both TOPCONS and MEMSAT-SVM algorithms, the biggest discrepancy being that neither model predicted any RLs. This is perhaps not surprising as, despite both TOPCONS and MEMSAT-SVM containing features to identify RLs, the accuracy of predicting such regions is significantly lower (22,31). Furthermore, we do

not know to which class of RL they belong (31) nor indeed if the RLs actually enter the membrane at all or rather form some globular domain.

To date, the topology of two other members of the MBOAT family of proteins that acylate proteins, Gup1p and GOAT, have been examined in any great detail. Both had complex models that were, however, similar to the HHAT topology in our study. Gup1p, a yeast protein that acylates (with C26:0) GPI-anchored proteins, was found to have 9TMs and 3 RLs (32), while GOAT recently was shown to contain 11TMs and 1RL (21). In both cases, the invariable His residue was luminal and the conserved Asn was cytosolic, similar to what we observe for HHAT, further enhancing the theory that all MBOATs have this structure for their proposed active sites (21,32,33). HHAT is unusual compared to the other MBOAT proteins, in that mutation of the invariable His residue of the MBOAT region does not completely abolish catalytic activity of the protein (Figure 8A) (13). This suggests that HHAT may function in a different manner to other members of the family. However, our model does not indicate, at least from a topological point of view, that the active site is different from that of Gup1p or GOAT. Alternatively, substrate specificity may underlie this difference; GOAT and Gup1 acylate serine and glycerol, respectively, both oxygen nucleophiles, whereas HHAT acylates a thiol. His may act as base to enhance the nucleophilic character of the Ser hydroxyl group via activation/deprotonation, but in the case of HHAT the Shh cysteine may be a sufficiently good nucleophile to attack Palm-CoA without activation. However, similar to what has been shown for other MBOAT proteins, mutation of the conserved Asp in HHAT does abrogate function completely (Figure 8A) (13). The cytosolic location of this residue suggests that it is not directly involved with the palmitoylation of Hh proteins, and likely is involved with either substrate recognition or HHAT stability. Although Asp 339 is cytosolic, it is in the same loop as the palmitoylated Cys 324 which would insert into the bilayer and have the effect of bringing this loop back up to the membrane surface where Asp339 could interaction with substrates.

RLs can have multiple functions within proteins, especially in pore forming transport channels. In Aquaporins, two RLs are surrounded by 6 TMs, thus lining the channel and providing selectivity to the transporter specifically for water molecules (34), while in the Glutamate transport proteins, a RL determines substrate binding within the pore (35). RLs can also stabilise the subunits of different channels through electrostatic interactions (36). It will be important to examine whether RL6 in both GOAT and HHAT functions in substrate recognition, especially as the acyl-CoA is negatively charged and it may be possible that RLs can create regions of positive electrostatic potential to aid the interaction (36). These regions may also affect the formation of HHAT multimers; although GOAT is suggested to exist and function as a monomer (21), HHAT does form non-covalent dimers in cells (see Figure 6B) as well as when the protein is purified *in vitro* (data not shown). It is unclear if the protein functions as a monomer or as a dimer; however, recent studies in the DHHC PATs revealed that DHHC2 and DHHC3 form inactive dimers, and dimerisation is inhibited by the autoacylation (37).

Using metabolic labelling experiments and multiple Cys to Ala mutants of HHAT we further show that HHAT is S-palmitoylated on four cytosolic Cys residues. Surprisingly, the impaired activity mutant HHAT H379A is only weakly palmitoylated indicating that palmitoylation of HHAT is important for its function. This could imply that the role of His379 in HHAT would be that of a structural regulator in the protein rather than being involved in catalytic activity. Unlike the DHHC PATs, where the importance of the DHHC motif and particularly of the Cys residue of the motif to the acylation of their target proteins is better understood, very little is known about how the invariant His residue of the MBOAT proteins functions in catalysis of the acylation of lipids and proteins. In the DHHC PATs, autoacylation at the Cys residue of the motif occurs upon interaction with the acyl-CoA to form a transient acyl-enzyme transfer intermediate, before transferring the acyl group to the protein substrate (29). It is likely that HHAT's palmitoylation is not directly involved in the N-palmitoylation of Hh proteins in a comparable manner to DHHC proteins, because HHAT acylation sites and Hh acylation occur on opposite sides of the membrane. However, the palmitoylation of HHAT may modulate protein function and/or structure in other ways that ultimately may affect Hh protein palmitoylation.

A recent study showed that the closely related MBOAT protein PORCN, which attaches a palmitoleoyl moiety to the Wnt family of proteins, is also palmitoylated (38). This study suggested that PORCN was palmitoylated on a single Cys, conserved only in primates, specifically Cys187 of human PORCN, and that palmitoylation of PORCN resulted in a reduction of palmitoleoylation and activity of Wnt proteins (38). However, it is likely that multiple PORCN Cys residues are palmitoylated similar to the situation with HHAT, as mutation of Cys187 to an Ala did not completely abrogate PORCN palmitoylation (38). Furthermore, it is unclear how a primate-specific Cys in PORCN would modulate Wnt activity so radically, especially as the function of PORCN is completely conserved in mice, which don't have this Cys residue. Unlike PORCN, all Cys residues palmitoylated in HHAT are conserved in primates and other mammalian sequences, such as mice and rat (Figure S1). Significantly, mutation of the His residue of PORCN did not affect palmitoylation of the protein, suggesting that this is a unique feature for HHAT. This result, when taken in consideration with the data that show that HHAT is the only known MBOAT in which mutation of the His residue still retains some activity of the protein, may suggest that HHAT does function in an unique manner compared to other MBOAT proteins.

Unlike the N-palmitoylation of Hh proteins, S-palmitoylation is catalysed by the DHHC PATs and attaches palmitic acid to proteins via thioester linkages to cysteine residues. This is a reversible process, via the function of the acyl-protein thioesterases (APTs), and as such it can be considered an "on-off" switch similar to protein phosphorylation (39). Palmitoylation of membrane proteins has been shown to affect association with other proteins (40), or the targeting of ER membrane proteins to specific domains within the ER membrane (41). HHAT palmitoylation could potentially have a similar effect on the protein. Future studies, perhaps with mass spectrometry analysis of HHAT-associated proteins or super-resolution microscopy of HHAT mutants, should provide clues to both possibilities. Insertion of the palmitates into the cytoplasmic leaflet of the ER may also locally affect membrane curvature to aid in interaction with the acyl-CoA or Hh substrates.

Another potential function is that palmitoylation affects the structure of HHAT. Palmitoylation of model proteins with a single TM in residues adjacent to the TM, disrupts the orientation of the helices within a lipid bilayer (42). Palmitoylation of HHAT may effect the tilting of the TMs within the ER membrane, thus affecting protein function. Repeating the experiments presented in this study with palmitoylation-deficient mutants of HHAT and seeing if topology is altered could test this hypothesis.

The result that the H379A mutant is not palmitoylated would perhaps suggest that the protein is actually autoacylated. However, due to the fact that the D339N HHAT mutant is only weakly active and yet still fully palmitoylated, it is likely that HHAT palmitoylation is not caused by autoacylation of the protein. Thus, identification of the DHHC PAT responsible for HHAT palmitoylation, as well as the interplay with the APTs, may provide a further dimension of how this protein is regulated by palmitoylation.

Finally, during mPEG accessibility analysis on the HHAT Cys mutants, an unexpected result was seen with the C324A mutant, the mPEG labelling produced significantly more bands, with a laddering effect of differentially tagged HHAT proteins (Figure 6C). The increase in molecular weight could be attributed to increased multimerisation of the protein. It is still unclear if MBOAT family proteins form functional multimers within the cell, although studies on GOAT suggest that the protein functions as a monomer (21). Intriguingly, this result could further suggest that the protein conformation is significantly altered in this protein, as more Cys residues within the protein are more accessible. The importance of this Cys residue is emphasised by the facts that it is the only Cys residue completely conserved in all examined species (Figure S1), and that it is also palmitoylated (Figure 7). Further studies with this mutant should reveal more as to its importance in regulating HHAT function.

In summary, we provide a comprehensive analysis of HHAT topology, showing that the protein consists of 10 TMs and 2 RLs, with the His residue of the proposed catalytic site facing the lumen of the ER. We provide evidence that HHAT is palmitoylated on multiple Cys residues on the cytoplasmic side of the protein and that mutation of the invariant His residue of the MBOAT domain affects palmitoylation of HHAT, while also showing that Cys324 of the protein may be important for controlling its

folding. From this study, it is clear that HHAT is an extremely complex protein with multiple factors affecting its function. This study provides the foundation upon which to build an understanding to how HHAT functions and how it may be inhibited, as well as creating new avenues of inquiry for future studies in this important class of proteins.

REFERENCES

1. McMahon, A. P., Ingham, P. W., and Tabin, C. J. (2003) Developmental roles and clinical significance of hedgehog signaling. *Curr Top Dev Biol* **53**, 1-114
2. Ingham, P. W., and McMahon, A. P. (2001) Hedgehog signaling in animal development: paradigms and principles. *Genes Dev* **15**, 3059-3087
3. Barakat, M. T., Humke, E. W., and Scott, M. P. (2010) Learning from Jekyll to control Hyde: Hedgehog signaling in development and cancer. *Trends in molecular medicine* **16**, 337-348
4. Scales, S. J., and de Sauvage, F. J. (2009) Mechanisms of Hedgehog pathway activation in cancer and implications for therapy. *Trends in pharmacological sciences* **30**, 303-312
5. Mann, R. K., and Beachy, P. A. (2004) Novel lipid modifications of secreted protein signals. *Annu Rev Biochem* **73**, 891-923
6. Chamoun, Z., Mann, R. K., Nellen, D., von Kessler, D. P., Bellotto, M., Beachy, P. A., and Basler, K. (2001) Skinny hedgehog, an acyltransferase required for palmitoylation and activity of the hedgehog signal. *Science* **293**, 2080-2084
7. Pepinsky, R. B., Zeng, C., Wen, D., Rayhorn, P., Baker, D. P., Williams, K. P., Bixler, S. A., Ambrose, C. M., Garber, E. A., Miatkowski, K., Taylor, F. R., Wang, E. A., and Galdes, A. (1998) Identification of a palmitic acid-modified form of human Sonic hedgehog. *J Biol Chem* **273**, 14037-14045
8. Callejo, A., Torroja, C., Quijada, L., and Guerrero, I. (2006) Hedgehog lipid modifications are required for Hedgehog stabilization in the extracellular matrix. *Development* **133**, 471-483
9. Chen, M. H., Li, Y. J., Kawakami, T., Xu, S. M., and Chuang, P. T. (2004) Palmitoylation is required for the production of a soluble multimeric Hedgehog protein complex and long-range signaling in vertebrates. *Genes Dev* **18**, 641-659
10. Buglino, J. A., and Resh, M. D. (2008) Hhat is a palmitoylacyltransferase with specificity for N-palmitoylation of Sonic Hedgehog. *J Biol Chem* **283**, 22076-22088
11. Chang, S. C., and Magee, A. I. (2009) Acyltransferases for secreted signalling proteins (Review). *Mol Membr Biol* **26**, 104-113
12. Hofmann, K. (2000) A superfamily of membrane-bound O-acyltransferases with implications for wnt signaling. *Trends Biochem Sci* **25**, 111-112
13. Buglino, J. A., and Resh, M. D. (2010) Identification of conserved regions and residues within Hedgehog acyltransferase critical for palmitoylation of Sonic Hedgehog. *PLoS One* **5**, e11195
14. Rodriguez-Blanco, J., Schilling, N. S., Tokhunts, R., Giambelli, C., Long, J., Liang Fei, D., Singh, S., Black, K. E., Wang, Z., Galimberti, F., Bejarano, P. A., Elliot, S., Glassberg, M. K., Nguyen, D. M., Lockwood, W. W., Lam, W. L., Dmitrovsky, E., Capobianco, A. J., and Robbins, D. J. (2013) The hedgehog processing pathway is required for NSCLC growth and survival. *Oncogene* **32**, 2335-2345
15. Konitsiotis, A. D., Chang, S. C., Jovanović, B., Ciepla, P., Masumoto, N., Palmer, C. P., Tate, E. W., Couchman, J. R., and Magee, A. I. (2014) Attenuation of hedgehog acyltransferase-catalyzed sonic hedgehog palmitoylation causes reduced signaling, proliferation and invasiveness of human carcinoma cells. *PLoS One* **9**, e89899
16. Petrova, E., Rios-Esteves, J., Ouerfelli, O., Glickman, J. F., and Resh, M. D. (2013) Inhibitors of Hedgehog acyltransferase block Sonic Hedgehog signaling. *Nat Chem Biol* **9**, 247-249
17. Heal, W. P., Jovanovic, B., Bessin, S., Wright, M. H., Magee, A. I., and Tate, E. W. (2011) Bioorthogonal chemical tagging of protein cholesterylation in living cells. *Chem Commun (Camb)* **47**, 4081-4083
18. Krogh, A., Larsson, B., von Heijne, G., and Sonnhammer, E. L. (2001) Predicting transmembrane protein topology with a hidden Markov model: application to complete genomes. *J Mol Biol* **305**, 567-580

19. Tsirigos, K. D., Hennerdal, A., Käll, L., and Elofsson, A. (2012) A guideline to proteome-wide α-helical membrane protein topology predictions. *Proteomics* **12**, 2282-2294
20. Bernsel, A., Viklund, H., Hennerdal, A., and Elofsson, A. (2009) TOPCONS: consensus prediction of membrane protein topology. *Nucleic Acids Res* **37**, W465-468
21. Taylor, M. S., Ruch, T. R., Hsiao, P. Y., Hwang, Y., Zhang, P., Dai, L., Huang, C. R., Berndsen, C. E., Kim, M. S., Pandey, A., Wolberger, C., Marmorstein, R., Machamer, C., Boeke, J. D., and Cole, P. A. (2013) Architectural organization of the metabolic regulatory enzyme ghrelin O-acyltransferase. *J Biol Chem* **288**, 32211-32228
22. Nugent, T., and Jones, D. T. (2009) Transmembrane protein topology prediction using support vector machines. *BMC Bioinformatics* **10**, 159
23. Pruitt, K. D., Brown, G. R., Hiatt, S. M., Thibaud-Nissen, F., Astashyn, A., Ermolaeva, O., Farrell, C. M., Hart, J., Landrum, M. J., McGarvey, K. M., Murphy, M. R., O'Leary, N. A., Pujar, S., Rajput, B., Rangwala, S. H., Riddick, L. D., Shkeda, A., Sun, H., Tamez, P., Tully, R. E., Wallin, C., Webb, D., Weber, J., Wu, W., DiCuccio, M., Kitts, P., Maglott, D. R., Murphy, T. D., and Ostell, J. M. (2014) RefSeq: an update on mammalian reference sequences. *Nucleic Acids Res* **42**, D756-763
24. Hofmann, K., and Stoffel, W. (1993) TMBASE - A database of membrane spanning protein segments. Biol. Chem. Hoppe-Seyler
25. Petersen, T. N., Brunak, S., von Heijne, G., and Nielsen, H. (2011) SignalP 4.0: discriminating signal peptides from transmembrane regions. *Nat Methods* **8**, 785-786
26. Le Gall, S., Neuhof, A., and Rapoport, T. (2004) The endoplasmic reticulum membrane is permeable to small molecules. *Mol Biol Cell* **15**, 447-455
27. Schrag, J. D., Bergeron, J. J., Li, Y., Borisova, S., Hahn, M., Thomas, D. Y., and Cygler, M. (2001) The Structure of calnexin, an ER chaperone involved in quality control of protein folding. *Mol Cell* **8**, 633-644
28. Ou, W. J., Bergeron, J. J., Li, Y., Kang, C. Y., and Thomas, D. Y. (1995) Conformational changes induced in the endoplasmic reticulum luminal domain of calnexin by Mg-ATP and Ca2+. *J Biol Chem* **270**, 18051-18059
29. Jennings, B. C., and Linder, M. E. (2012) DHHC protein S-acyltransferases use similar ping-pong kinetic mechanisms but display different acyl-CoA specificities. *J Biol Chem* **287**, 7236-7245
30. Forrester, M. T., Hess, D. T., Thompson, J. W., Hultman, R., Moseley, M. A., Stamler, J. S., and Casey, P. J. (2011) Site-specific analysis of protein S-acylation by resin-assisted capture. *J Lipid Res* **52**, 393-398
31. Viklund, H., Granseth, E., and Elofsson, A. (2006) Structural classification and prediction of reentrant regions in alpha-helical transmembrane proteins: application to complete genomes. *J Mol Biol* **361**, 591-603
32. Pagac, M., de la Mora, H. V., Duperrex, C., Roubaty, C., Vionnet, C., and Conzelmann, A. (2011) Topology of 1-acyl-sn-glycerol-3-phosphate acyltransferases SLC1 and ALE1 and related membrane-bound O-acyltransferases (MBOATs) of Saccharomyces cerevisiae. *J Biol Chem* **286**, 36438-36447
33. Pagac, M., Vazquez, H. M., Bochud, A., Roubaty, C., Knöpfli, C., Vionnet, C., and Conzelmann, A. (2012) Topology of the microsomal glycerol-3-phosphate acyltransferase Gpt2p/Gat1p of Saccharomyces cerevisiae. *Mol Microbiol* **86**, 1156-1166
34. Sui, H., Han, B. G., Lee, J. K., Walian, P., and Jap, B. K. (2001) Structural basis of water-specific transport through the AQP1 water channel. *Nature* **414**, 872-878
35. Slotboom, D. J., Sobczak, I., Konings, W. N., and Lolkema, J. S. (1999) A conserved serine-rich stretch in the glutamate transporter family forms a substrate-sensitive reentrant loop. *Proc Natl Acad Sci U S A* **96**, 14282-14287
36. Law, R. J., and Sansom, M. S. (2002) Water transporters: how so fast yet so selective? *Curr Biol* **12**, R250-252
37. Lai, J., and Linder, M. E. (2013) Oligomerization of DHHC Protein S-Acyltransferases. *J Biol Chem* **288**, 22862-22870
38. Gao, X., and Hannoush, R. N. (2014) Single-cell imaging of Wnt palmitoylation by the acyltransferase porcupine. *Nat Chem Biol* **10**, 61-68

39. Linder, M. E., and Deschenes, R. J. (2007) Palmitoylation: policing protein stability and traffic. *Nat Rev Mol Cell Biol* **8**, 74-84
40. Delandre, C., Penabaz, T. R., Passarelli, A. L., Chapes, S. K., and Clem, R. J. (2009) Mutation of juxtamembrane cysteines in the tetraspanin CD81 affects palmitoylation and alters interaction with other proteins at the cell surface. *Exp Cell Res* **315**, 1953-1963
41. Lakkaraju, A. K., Abrami, L., Lemmin, T., Blaskovic, S., Kunz, B., Kihara, A., Dal Peraro, M., and van der Goot, F. G. (2012) Palmitoylated calnexin is a key component of the ribosome-translocon complex. *EMBO J* **31**, 1823-1835
42. Joseph, M., and Nagaraj, R. (1995) Conformations of peptides corresponding to fatty acylation sites in proteins. A circular dichroism study. *J Biol Chem* **270**, 19439-19445

ACKNOWLEDGEMENTS
We thank Ms. Nino Gaphrindashvili for optimisation of the mPEG protocol, and Mr. Jianfei Feng and Mr. David Corcoran for production of some of the mutants used in this paper. We thank the FILM facility for access to microscopes and Mr. George Bodakh for performing some of the HHAT activity assays. This work was funded by grants to AIM and EWT from the Pancreatic Cancer Research Fund and Cancer Research UK. BJ was funded by a PhD studentship from the NHLI Foundation; PC was funded by a PhD studentship from the Imperial College London Institute of Chemical Biology EPSRC Centre for Doctoral Training (grant EP/F500416/1).

FOOTNOTES
Abbreviations: Hh, Hedgehog; HHAT, Hedgehog acyltransferase; PAT, protein acyltransferase; APT, acyl protein thioesterase; siRNA, small interfering RNA; TM, transmembrane domain; RL, re-entrant loop; ER, endoplasmic reticulum; MBOAT, membrane bound O-acyltransferase; PORCN, Porcupine; GOAT, Ghrelin-O-acyltransferase.

FIGURE 1. Bioinformatic prediction analysis of HHAT sequences identifies a maximum of 13 predicted transmembrane domains (TMs). Clustal Omega sequence alignment of human HHAT sequence with the TMs predictions from three separate bioinformatic algorithms: TOPCONS, MEMSAT-SVM and TMpred. Predicted TMs are highlighted in red and loops are numbered in accordance with the epitope insertion analysis from our experiments. The TMpred algorithm predicted a helix within loop 8, and so mutants were made at two places in the loop between predicted TMs 8 and 9, in order to accommodate this prediction. These mutants were numbered 8 and 8b. In all models, the critical His379 residue is predicted to be part of TM-9. Positions selected for epitope and TEV tag insertions used in this study are indicated with arrows. The diagrams below depict the predicted topologies from each of the algorithms, along with the predicted loop location. The black boxes depict the predicted TMs, while the lines depict the loop regions. Loops are coloured red and blue depending on if they were predicted to be luminal or cytosolic, respectively. In the MEMSAT-SVM diagram TMs 5, 6 and 8 were predicted to be pore-lining helices, which are depicted in magenta. Loops and TMs are not drawn exactly to scale, but do indicate relative size differences.

FIGURE 2. Mapping of HHAT topology by TEV cleavage of microsomal preparations. HHAT constructs containing a C-terminal V5-6xHis epitope tag and an internal TEV protease tag at indicated loops were transfected into HEK293a cells and intact microsomal preparations prepared by ultracentrifugation. **A.** In order to show that the microsomal preparations have intact ER membranes, mPEG, a hydrophilic reagent of 5 kDa that reacts with -SH groups, did not react with the non-disulphide-bonded cysteine in the ER luminal protein GRP94 when it was added to 10μg of the microsomal preparations (**A. I.**). After treatment of the microsomes with 0.2% Triton-X 100 (**A. II.**) GRP94 is modified by mPEG, and the reaction could be blocked by the reducing agent DTT (**A. III.**). GRP94* indicates the position of the modified proteins. **B.** Microsome preparations were treated with TEV-Buffer (**I**) or Pro-TEV protease (see Experimental procedures) (**II**) for 4h at 25^{o}C with agitation. Reaction was then stopped with sample buffer and samples analysed by SDS-PAGE and probed firstly with anti-V5 antibody, and then reprobed with anti-6xHis antibody. Because the microsomal preparations are intact, any TEV cleavage sites on luminal loops will be inaccessible to the Pro-TEV protease. However, any cytosolic sites will be accessible to the protease and so the protein will be cleaved and produce a shorter C-terminal fragment, which will be identified by antibody labelling. Using this method the HHAT topology model indicated below figure (**C. II.**) was produced; red lines indicate the TEV site was inaccessible and hence luminal, blue lines indicate the TEV site was accessible and hence cytoplasmic. Cleaved bands are indicated by black arrowheads, while grey arrowheads indicate potential cleaved products. It was unclear if mutants 1/2 and 2/3 produced any cleavage product. Immunoblots shown are representative results from 5 independent experiments. **D.** A construct containing the TEV protease tag in the linker sequence between the C-terminal V5 epitope and the 6xHis epitope tag was used to examine the topology of the C-terminus of HHAT. Specifically, if the C-terminus is cytosolic and accessible to TEV protease cleavage, reactivity of the protein with a 6xHis antibody would be lost after treatment with Pro-TEV, while reactivity with the

V5 antibody should be retained. This is what was observed in the experiments with this construct, indicating that the C-terminus is cytosolic.

FIGURE 3. Mapping of HHAT topology by V5 epitope indirect immunofluorescence in selectively permeabilised cells. HHAT constructs containing a C-terminal FLAG epitope tag and an internal V5 epitope tag at indicated loops were transfected into HeLa cells plated on 96-well imaging plates. Cell membranes were either permeabilised with 0.2% Triton-X 100 (TX100) or with 0.04% digitonin (Dig). Permeabilisation with digitonin maintains the ER membrane intact, while permeabilisation with Triton-X 100 fully permeabilises all the membranes of the cell. FLAG and V5 epitopes were stained with specific primary antibodies, followed by secondary antibodies with 555nm (red) or 488 (green) excitation wavelengths, respectively. To control for the selective permeabilisation of the ER membrane, untransfected cells were selectively permeabilised and stained for Calnexin using two different antibodies, one which binds to an epitope on the luminal N-terminus of the protein and another which bind to an epitope on the cytosolic C-terminus of the protein (**I**). Only two conditions are shown, for the V5 epitope in the N-terminus of the protein (**II**) and in predicted loop 1 (**III**). The N- and C-termini of HHAT were both cytosolic (**II**), thus the FLAG epitope will always be stained, regardless of detergent used for permeabilisation. Images were then analysed using Volocity image analysis software to determine the colocalisation coefficient of the two channels. Insets show higher magnification of indicated regions. The histogram (IV) shows mean Manders' coefficients (MC) for colocalisation of the red (555nm) channel with the green (488nm) channel for different HHAT mutants and for the Calnexin control (n>40 cells, error bars indicate the standard deviation). High Manders' coefficients indicate better colocalisation of FLAG-tagged proteins with V5-tagged proteins. Values less than 0.5 indicate low colocalisation. Identical exposures and image normalisation for both permeabilisations ensure fair side-by-side comparison. Schematics underneath panels II and III illustrate the positions of the stained epitopes. Images are examples of each condition from at least three independent experiments. Scale bars: 15μm.

FIGURE 4. N-glycosylation analysis of full length HHAT, HHAT-Δ157-493 and HHAT-Δ192-493 truncation mutants, containing a C-terminal N-glycosylation motif. *In vitro* translation/translocation of HHAT truncations ending in predicted loop regions 4 (Δ157-493 mutant) and 5 (Δ192-493 mutant), or full length HHAT cDNA, C-terminally tagged with an N-glycosylation site and a V5 epitope. Luminal N-glycosylation sites become glycosylated and the covalent attachment to the protein can be detected by a shift in molecular weight on an SDS-PAGE gel. Following expression, lysates were treated or not with PNGase F, an endoglycosidase which cleaves N-glycans between the innermost sugar moiety and Asn, removing the shift in molecular weight of glycosylated proteins. Lysates were analysed by SDS-PAGE on 7.5% gels, followed by immunoblotting with anti-V5 antibody. HHAT* indicates glycosylated HHAT protein.

FIGURE 5. HHAT topology experimental consensus model indicates 10 TMs and 2 re-entrant loops (RLs). Figure displays the consensus HHAT topology model including palmitoylation modifications, based on the data shown in the table below which summarises the results from the three different experiments, indicating if a loop is luminal (L) or cytoplasmic (C), the consensus model is indicated at the bottom. Our data indicate that predicted TM-3 and TM-6 are likely to be RLs. The cytosolic loops containing cysteines that are palmitoylated display the fatty acid modification as a bent line. Relative loop length is approximated by the size of the loops, but not precisely scaled; cytosolic loops are coloured blue and luminal loops red. Positions of the two conserved MBOAT residues, Asp339 and His379, are indicated with arrows.

FIGURE 6. HHAT cysteine mapping in selectively permeabilised cells. **A.** HEK293a cells expressing HHAT-V5-6xHis were permeabilised with 0.04% digitonin or 1% Triton X-100 as indicated. Modification was carried out for 30 min at 4°C with 1 mM mPEG. Samples were analysed by SDS-PAGE on 7.5% gels, followed by immunoblotting with antibodies to V5 (upper panel) or GRP94 (lower panel). **B.** HEK293a cells expressing the indicated HHAT single cysteine mutants were permeabilised with 1% Triton X-100. Modification was carried out for 30 min at 4°C with 1

mM mPEG; where indicated, DTT was present during the reaction. Samples were analysed by SDS-PAGE on 7.5% gels, followed by immunoblotting with antibodies to V5 (upper panels) or GRP94 (lower panels). Immunoblots shown are representative results from 4 independent experiments. **C.** HEK293a cells expressing HHAT C324A mutant were permeabilised with 1% Triton X-100. Modification was carried out for 30 min at 4°C with 1 mM mPEG; where indicated, DTT was present during the reaction. Samples were analysed by SDS-PAGE on 7.5% gels, followed by immunoblotting with antibodies to V5 (upper panel) or GRP94 (lower panel). HHAT* and GRP94* indicate the positions of the modified proteins.

FIGURE 7. HHAT is palmitoylated on multiple cysteines via thioester linkage. **A.** HEK293a cells were transfected with a construct expressing the WT human HHAT cDNA C-terminally tagged with V5 and 6xHis epitopes. Cells were then fed overnight with 50μM palmitic acid analogue with a clickable alkyne moiety (YnPalm) or with vehicle (0.1% DMSO). Cells were lysed and HHAT was immunoprecipitated (IP) using anti-V5 antibody. Immunoprecipitated proteins or lysates were ligated by CuAAC to AzTB. Tagged proteins were separated on 15% SDS-PAGE gels and analysed by in-gel fluorescence (upper panels) and immunoblotting with antibody against 6xHis (lower panels). **B.** Lysates were prepared as in previous experiment; however, before immunoprecipitation lysates were either treated with 1M NH2OH pH 7.5 or 1M Tris pH 7.5 for 5h at room temperature, as described in the materials and methods section. Lysates were then precipitated by chloroform/methanol precipitation, resolubilised in 0.2% Triton X100 in PBS, immunoprecipitated with αV5 antibody, ligated by CuAAC to AzTB and analysed by SDS-PAGE in-gel fluorescence (upper panel) and anti-6xHis immunoblotting (lower panel). **C.** HEK293a cells were transfected with constructs expressing WT human HHAT cDNA, the luminal cysteine mutant HHAT-LumCys, or the cytosolic cysteine mutants HHAT-3CysA or HHAT-4CysA. Cells were then fed overnight with 50μM YnPalm or 0.1% DMSO. Cells were then lysed, immunoprecipitated with anti-V5 antibody, ligated by CuAAC to AzTB and analysed by SDS-PAGE in-gel fluorescence (upper panels) and anti-6xHis immunoblotting (lower panels).

FIGURE 8. His379 is implicated in HHAT palmitoylation. **A.** HHAT activity for the D339N and H379A mutants was determined by measuring the ability of the purified and solubilised HHAT mutant proteins to palmitoylate a Shh peptide, using an in-house developed *in vitro* click-chemistry based palmitoylation assay. HHAT-D339N-V5-6xHis showed only ~3% activity compared to WT, while HHAT-H379A-V5-6xHis mutant had ~63% activity compared to WT. Data are presented as mean ± SD and normalised to HHAT-WT-V5-6xHis. **B.** HEK293a cells were transiently transfected with HHAT-D339N-V5-6xHis or HHAT-H379A-V5-6xHis mutant constructs. Cells were then fed overnight with 50μM YnPalm or with 0.1% DMSO. Cells were lysed and HHAT was immunoprecipitated using a V5 antibody. Immunoprecipitated proteins or lysates were ligated by CuAAC to AzTB. Tagged proteins were separated on 15% SDS-PAGE gels and analysed by in-gel fluorescence (upper panel) and immunoblotting with antibody against the His tag (lower panel). Gels and immunoblots shown are representative results from 2 independent experiments.

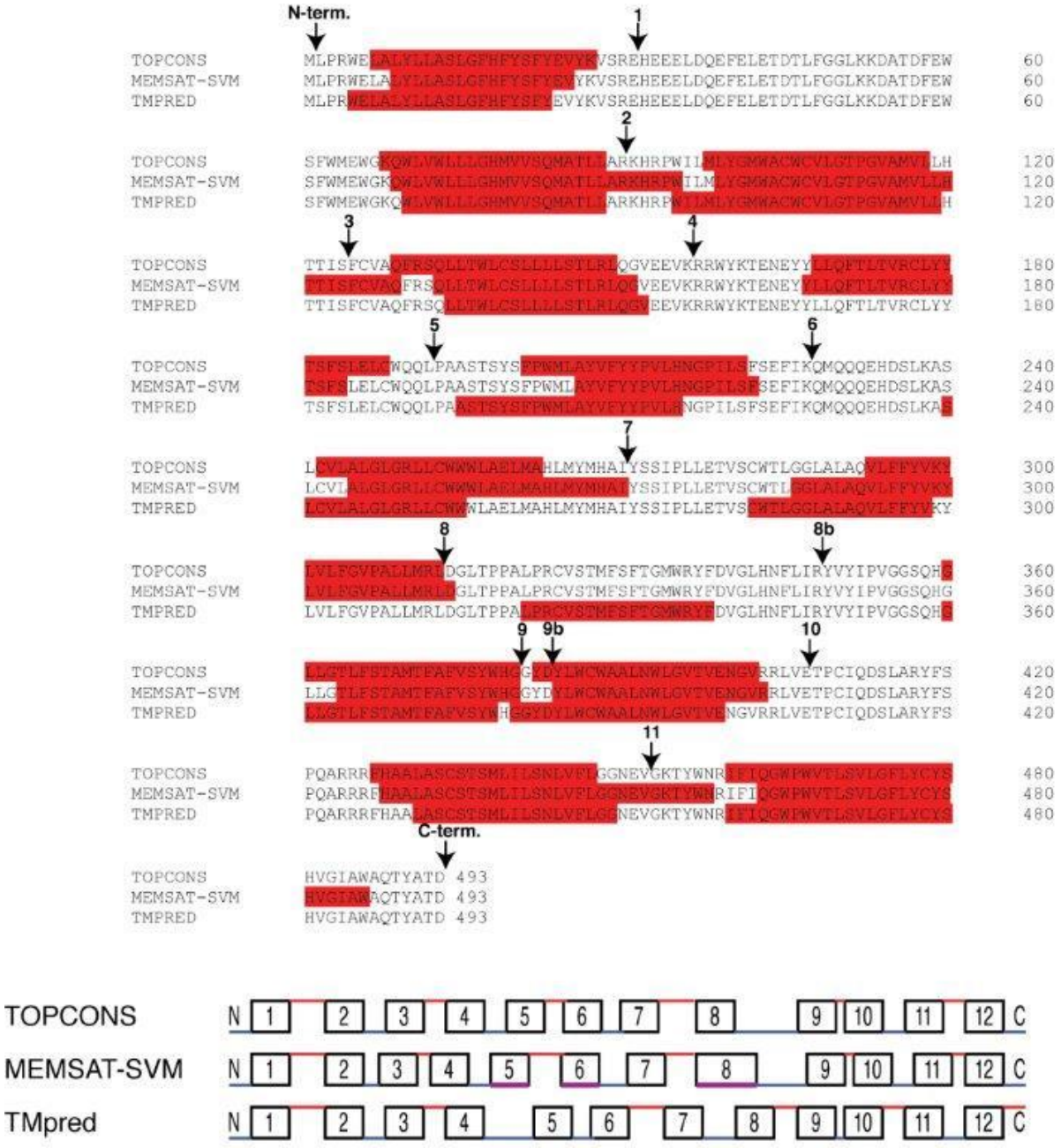
N-term.
1
2
3
4
5
6
7
8
8b
9
9b
10
11
C-term.
TOPCONS
MEMSAT-SVM
TMPRED
TOPCONS
N 1 2 3 4 5 6 7 8 9 10 11 12 C
MEMSAT-SVM
N 1 2 3 4 5 6 7 8 9 10 11 12 C
TMpred
N 1 2 3 4 5 6 7 8 9 10 11 12 C

Figure 1

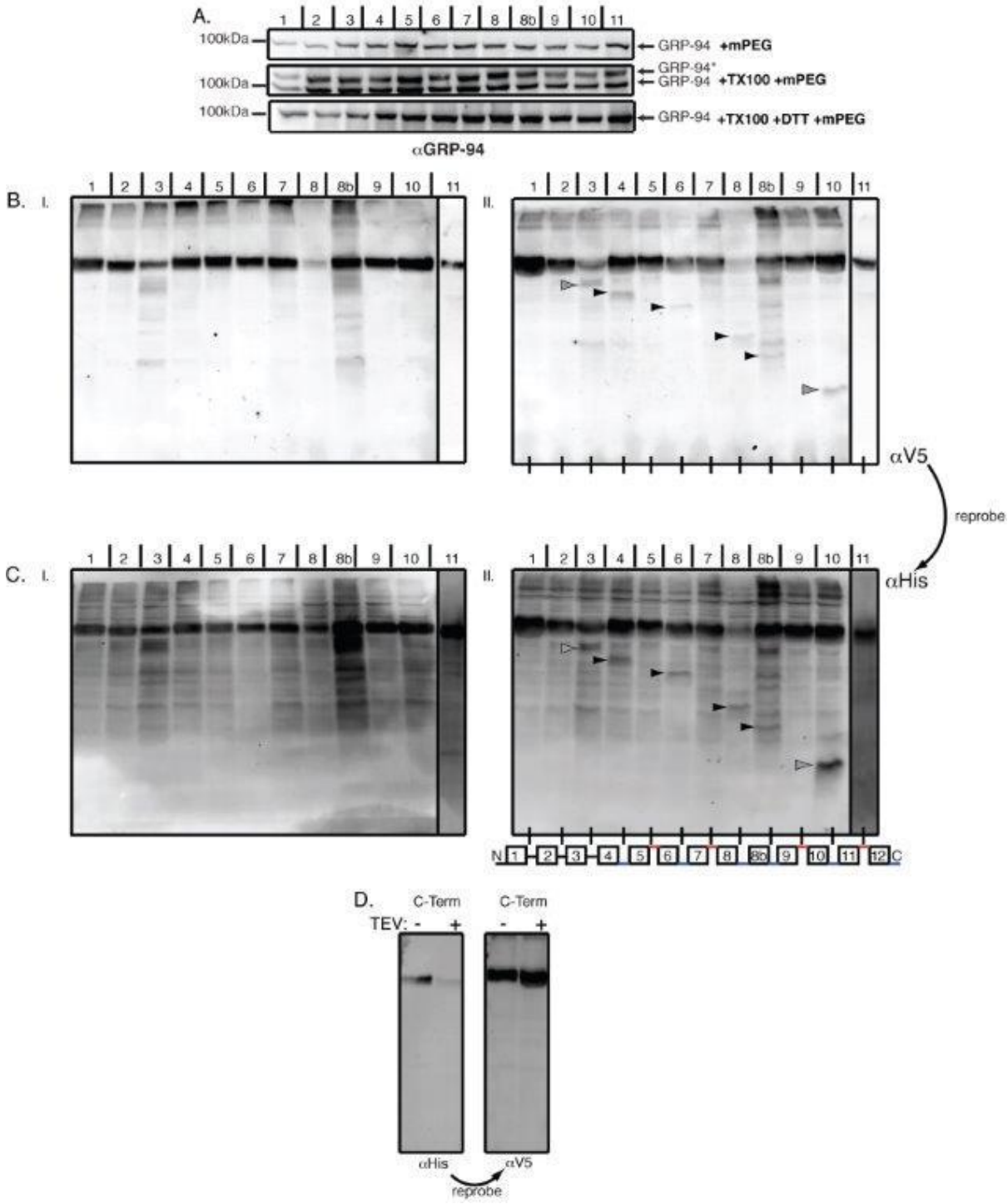
A.
1 2 3 4 5 6 7 8 8b 9 10 11
100kDa
GRP-94 +mPEG
GRP-94*
GRP-94 +TX100 +mPEG
100kDa
GRP-94 +TX100 +DTT +mPEG
100kDa
αGRP-94
B. I.
II.
αV5
reprobe
C. I.
II.
αHis
N 1 2 3 4 5 6 7 8 8b 9 10 11 12 C
D.
C-Term
C-Term
TEV: - + - +
αHis
αV5
reprobe

Figure 2

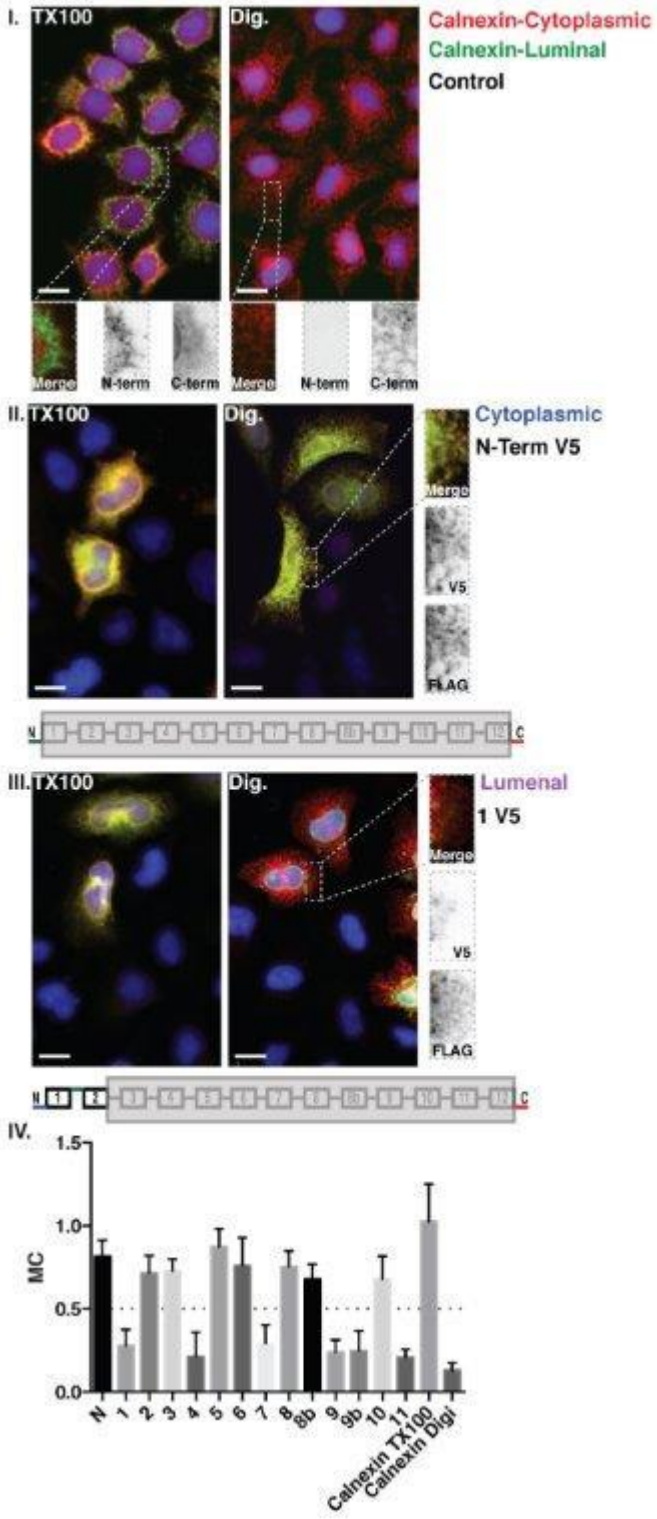
I.
TX100
Dig.
Calnexin-Cytoplasmic
Calnexin-Luminal
Control
Merge
N-term
C-term
II.
Cytoplasmic
N-Term V5
V5
FLAG
III.
Lumenal
1 V5
IV.
MC
1.5
1.0
0.5
0.0
N 1 2 3 4 5 6 7 8 8b 9 9b 10 11
Calnexin TX100
Calnexin Digi

Figure 3

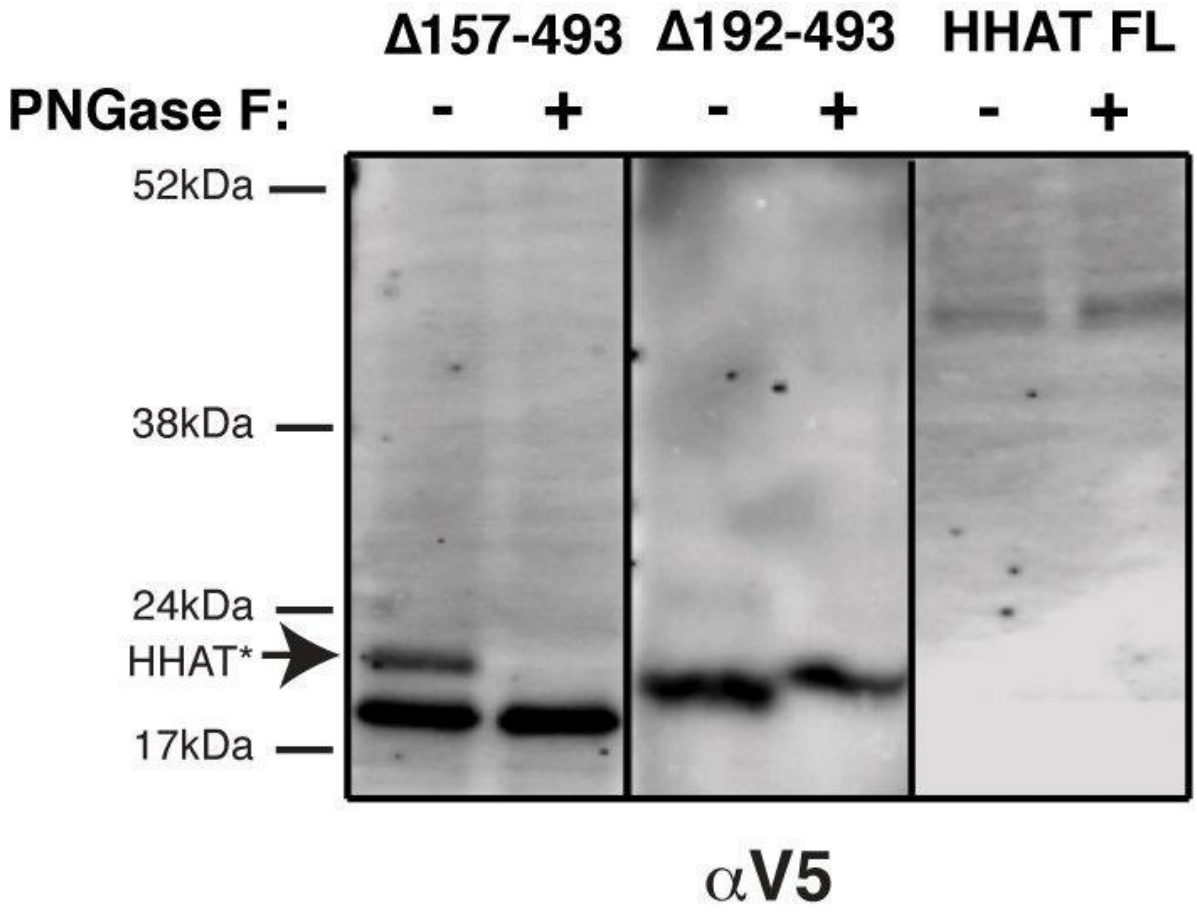
Δ157-493
Δ192-493
HHAT FL
PNGase F:
- + - + - +
52kDa
38kDa
24kDa
HHAT*
17kDa
αV5

Figure 4

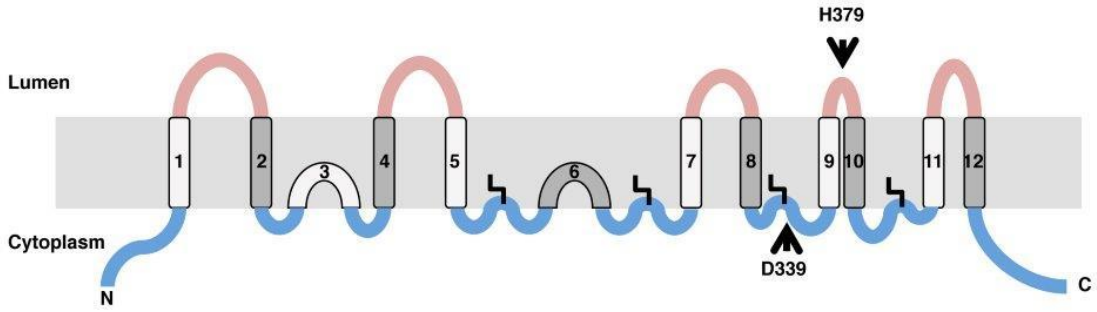

	N-Term	L1	L2	RL3	L4	L5	RL6	L7	L8	L8b	L9	L10	L11	C-Term
TEV	N/A	N/A	N/A	C(?)	C	L	C	L	C	C(?)	L	C	L	C
V5	C	L	C	C	L	C	C	L	C	C	L	C	L	C
Glyco	N/A	N/A	N/A	N/A	L	C	N/A	N/A	N/A	N/A	N/A	N/A	N/A	C
Cons	**C**	**L**	**C**	**C**	**L**	**C**	**C**	**L**	**C**	**C**	**L**	**C**	**L**	**C**

Figure 5

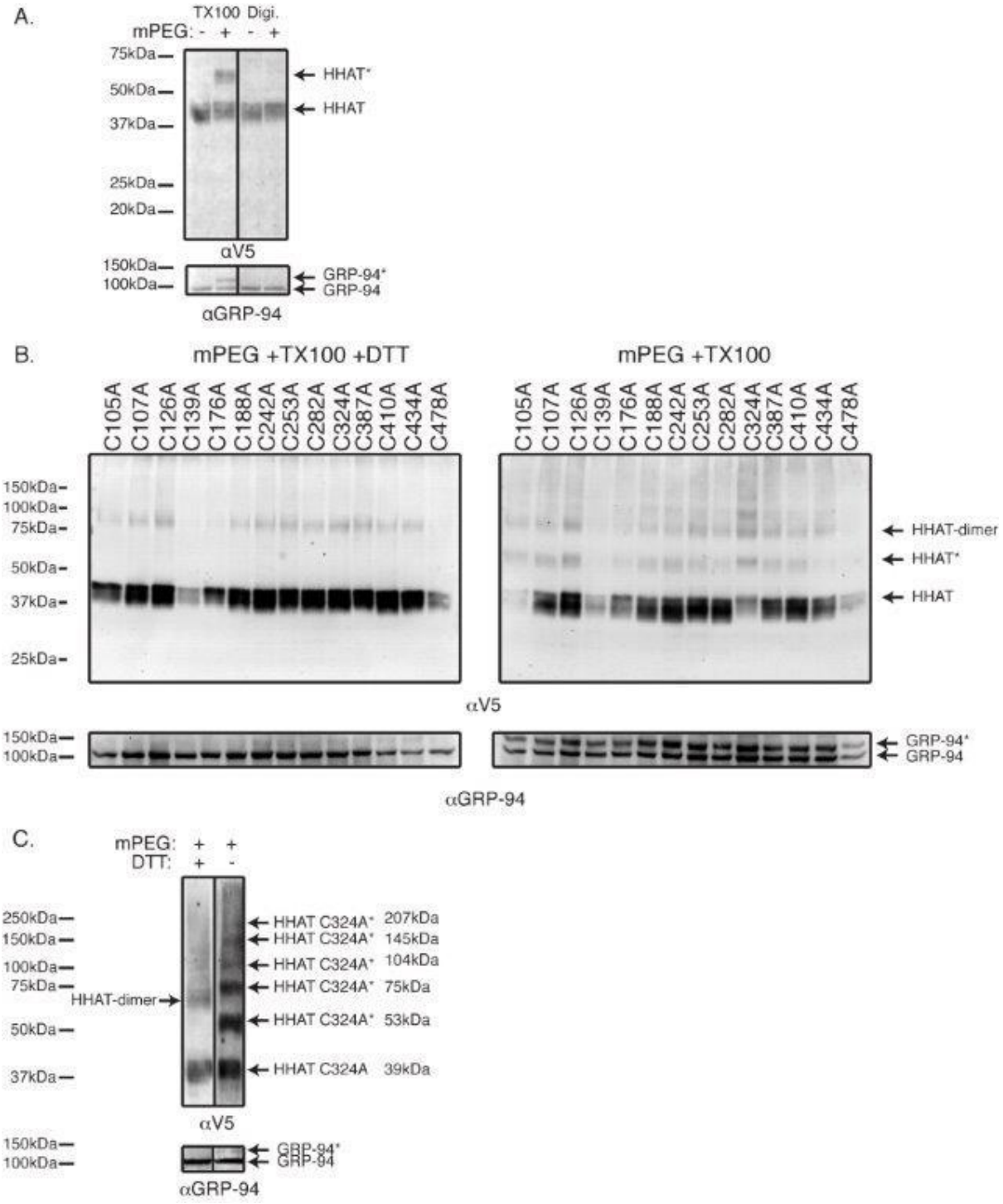
A.
TX100 Digi.
mPEG: - + - +
75kDa
50kDa
37kDa
25kDa
20kDa
HHAT*
HHAT
αV5
150kDa
100kDa
GRP-94*
GRP-94
αGRP-94
B.
mPEG +TX100 +DTT
mPEG +TX100
C105A C107A C126A C139A C176A C188A C242A C253A C282A C324A C387A C410A C434A C478A
150kDa
100kDa
75kDa
50kDa
37kDa
25kDa
HHAT-dimer
HHAT*
HHAT
αV5
GRP-94*
GRP-94
αGRP-94
C.
mPEG: + +
DTT: + -
250kDa
150kDa
100kDa
75kDa
50kDa
37kDa
HHAT-dimer
HHAT C324A* 207kDa
HHAT C324A* 145kDa
HHAT C324A* 104kDa
HHAT C324A* 75kDa
HHAT C324A* 53kDa
HHAT C324A 39kDa
αV5
GRP-94*
GRP-94
αGRP-94

Figure 6

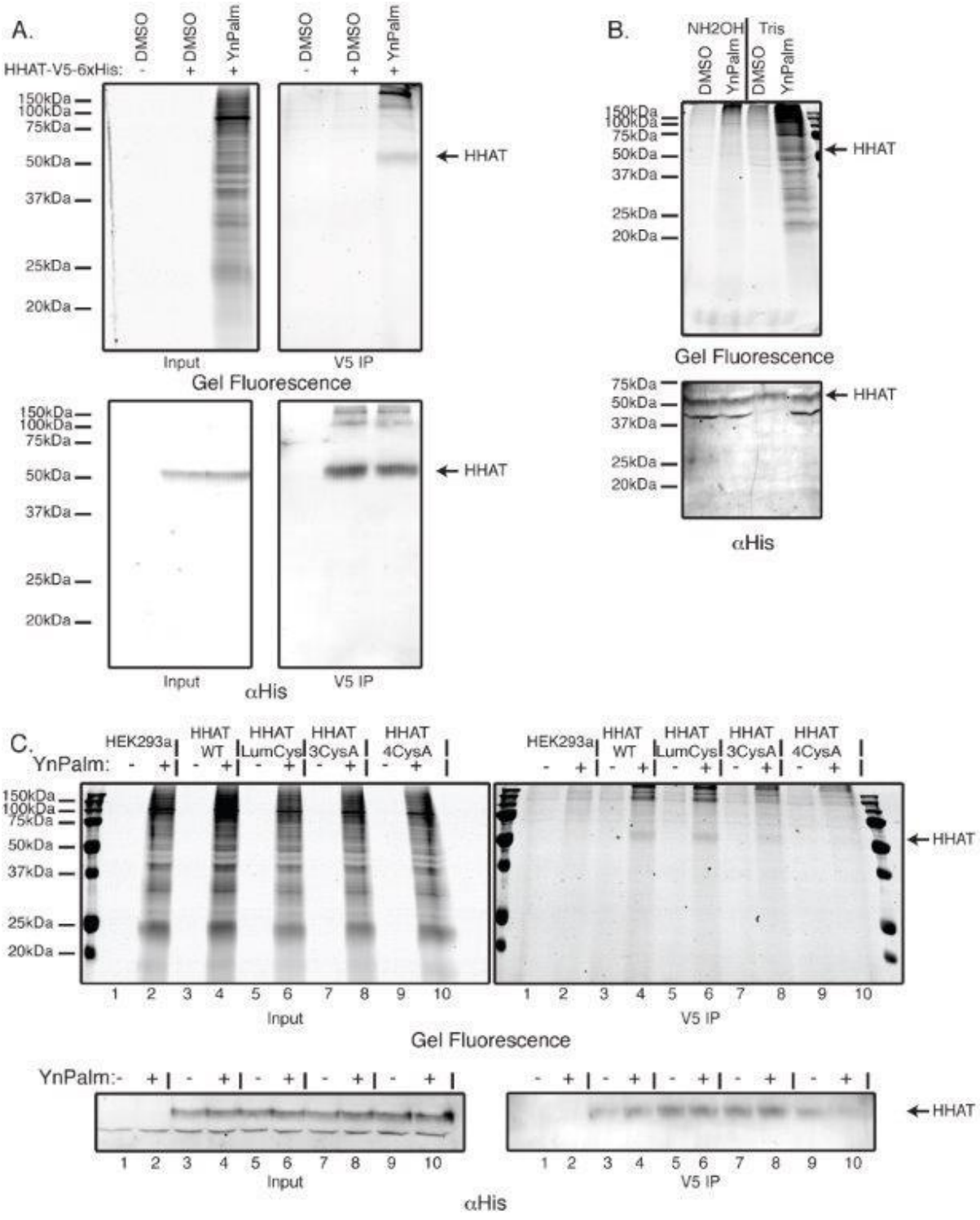
A.
HHAT-V5-6xHis:
DMSO
DMSO
YnPalm
DMSO
DMSO
YnPalm
150kDa
100kDa
75kDa
50kDa
37kDa
25kDa
20kDa
HHAT
Input
V5 IP
Gel Fluorescence
αHis
B.
NH2OH
Tris
DMSO
YnPalm
DMSO
YnPalm
C.
HEK293a
HHAT WT
HHAT LumCys
HHAT 3CysA
HHAT 4CysA
YnPalm:
Input
V5 IP
Gel Fluorescence
αHis

Figure 7

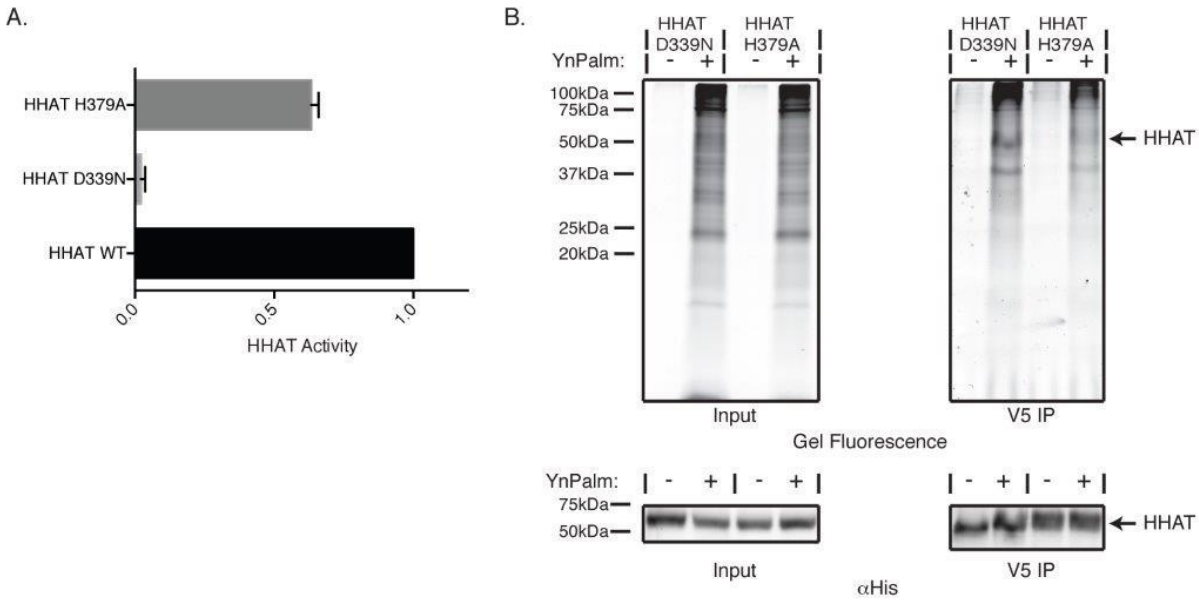
A.
HHAT H379A
HHAT D339N
HHAT WT
0.0
0.5
1.0
HHAT Activity
B.
HHAT D339N
HHAT H379A
YnPalm:
- + - +
100kDa
75kDa
50kDa
37kDa
25kDa
20kDa
HHAT
Input
V5 IP
Gel Fluorescence
YnPalm:
75kDa
50kDa
HHAT
Input
V5 IP
αHis

Figure 8

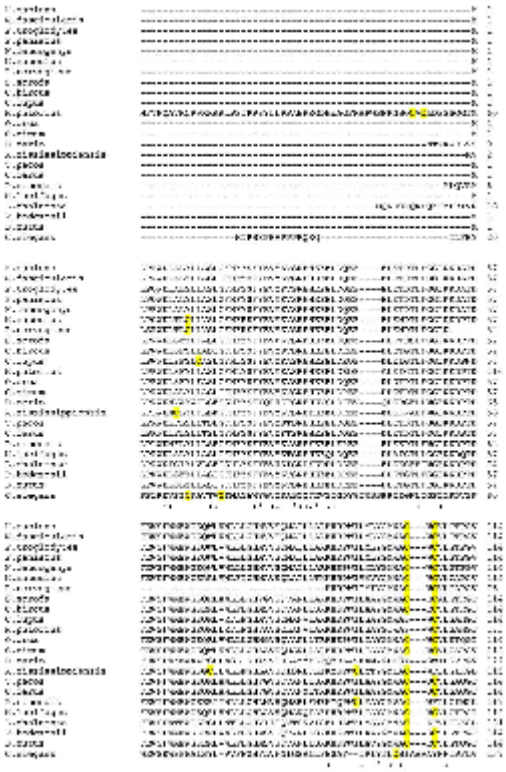

Supplementary Figure 1